Guest Ion Recognition and Energy Migration/Transfer in a Supramolecular Cubic Assembly of Tetrakis(rubidium 18-crown-6) Tetrachloromanganate(II) Species

Richard A. Fairman, Winklet A. Gallimore, Kirk V. N. Spence, and Ishenkumba A. Kahwa*

Chemistry Department, University of the West Indies, Mona, Kingston 7, Jamaica

Received October 20, 1992®

Competitive complexation of MCl_4^{2-} ligands (M = Mn, Fe, Co, Ni, Cu, Zn) to yield cubic *F*23 $[(Rb18C6)_4\{(MnCl_4)_{1-x}(MCl_4)_x\}][TlCl_4]_2$ complexes and the luminescence decay dynamics of the trapped $[(Rb18C6)_4MnCl_4]^{2+}$ species were studied. The results reveal sensitivity of the supramolecular cubic lattice to variations in the thermodynamic stability of T_d MCl_4^{2-} anions. Extensive multipolar interactions along the $[(Rb18C6)_4MnCl_4]^{2+}$ sublattice are evident from facile donor–donor energy transfer. For $[(A18C6)_4MnCl_4][TlCl_4]_2$ (A = Rb, Tl), energy migration terminates in thermalized (≈50 kJ mol^{-1}) exciton trapping by water molecules, presumably present in $[(A18C6)_4MnCl_4][TlCl_4]_2{\cdot}0.25H_2O$ impurities. The thermal barrier is attributed to the dynamic reorientational motion of 18C6, which exhibits a similar thermal barrier. For $[(Rb18C6)_4\{(MnCl_4)_{1-x}(CuCl_4)_x\}][TlCl_4]_2$ compounds, diffusive energy transfer from $[(Rb18C6)_4MnCl_4]^{2+}$ to $[(Rb18C6)_4CuCl_4]^{2+}$ traps dominates. Assuming dominant dipole–dipole interactions, the Cu^{2+}–Mn^{2+} and Mn^{2+}–Mn^{2+} coupling constants are 2.4×10^{-50} M^6 s^{-1} and 1.1×10^{-52} M^6 s^{-1}, respectively.

Introduction

The thallium-rich complexes $[(Tl18C6)_4MCl_4][TlCl_4]_2{\cdot}nH_2O$[1] [M = Cu, *n* = 0 (**1**); M = Cu, *n* = 0.25 (**2**); M = Mn, *n* = 0 (**3**)], $[(Tl18C6)_4CuBr_4][TlBr_4]_2$ (**4**),[2] and the rubidium isomorph $[(Rb18C6)_4MCl_4][TlCl_4]_2$ (**5**, M = Cu) crystallize in the cubic *F*23 form. The transition metal complex anionic ligands MCl_4^{2-}, M = Mn, Cu, and Zn, play an important role of concentrating the thallium(I) ions. Four $Tl18C6^+$ species are coordinated to each MCl_4^{2-} ligand, and the resulting complex $[(Tl18C6)_4MCl_4]^{2+}$ cations interact with highly thermodynamically stable $TlCl_4^-$ counteranions to yield the cubic *F*23 lattices of **1**–**3** and **5**. Understanding the factors which influence the formation and stabilization of these thallium-rich supramolecular[4-15] complexes is essential for the exploration of their potential applications in the extractive metallurgy of toxic thallium.[3] But more significantly, the family of compounds **1**–**5** is important for investigations of guest–host interactions and molecular recognition events in which supramolecular assemblies are formed and stabilized by a series of interactions operating in tandem.[4-15] For example, the formation of $[(Rb18C6)_4MnCl_4][TlCl_4]_2$, M = Mn, Co, Ni, Cu, and Zn, requires several processes (with solvent molecules omitted):

$$Rb^+ + 18C6 \rightleftharpoons Rb18C6^+ \quad \text{(i)}$$

$$M(OH_2)_6^{2+} + 4Cl^- \rightleftharpoons MCl_4^{2-} + 6H_2O \quad \text{(ii)}$$

$$4Rb18C6^+ + MCl_4^{2-} \rightleftharpoons [(Rb18C6)_4MnCl_4]^{2+} \quad \text{(iii)}$$

$$[(Rb18C6)_4MnCl_4]^{2+} + 2TlCl_4^- \rightleftharpoons [(Rb18C6)_4MCl_4][TlCl_4]_2 \quad \text{(iv)}$$

The thallium analogues **1**–**3** require an additional reversible oxidation step[1] for the formation of $TlCl_4^-$:

$$Tl18C6^+ + 4Cl^- \rightleftharpoons TlCl_4^- + 18C6 + 2e \quad \text{(v)}$$

Significant information is available on processes i[16] and ii[17] but the factors contributing to the progress of the thallium redox, v, and rubidium/thallium enrichment, iii and iv, reactions are unknown. It was therefore interesting to study the influence of well-known variations in the thermodynamic stability of MCl_4^{2-} ions on the thallium enrichment processes in iii and iv. We herein report the preparation and photophysical properties of $[(Rb18C6)_4\{(MnCl_4)_{1-x}(MCl_4)_x\}][TlCl_4]_2$ (**6**).

Experimental Details

Sample Preparation. Large good quality crystals of the complexes studied were readily grown by slow evaporation of ethanolic/butanolic solutions of rubidium chloride, 18C6, thallium(III) chloride, and appropriate transition metal chlorides as described previously.[1,2] $NiCl_2{\cdot}6H_2O$ (purified, from J. T. Baker), $FeCl_2$ (from metallic iron powder from J. T. Baker), and $CoCl_2{\cdot}6H_2O$ (Analar from BDH) were additional

® Abstract published in *Advance ACS Abstracts,* January 15, 1994.

(1) Kahwa, I. A.; Miller, D.; Mitchell, M.; Fronczek, F. R.; Goodrich, R. G.; Williams, D. J.; O'Mahoney, E. A.; Slawin, A. M. Z.; Ley, S. V.; Groombridge, C. J. *Inorg. Chem.* **1992**, *31*, 3963.
(2) Kahwa, I. A.; Miller, D.; Mitchell, M.; Fronczek, F. R. *Acta Crystallogr., Sect. C: Cryst. Struct. Commun.* **1993**, *49*, 320.
(3) Sanderson, L. *Can. Miner. J.* **1964**, *65*, 624. Prater, J. D.; Schlain, D.; Ravitz, S. F. Recovery of Thallium from Smelter Products. *U.S. Bur. Mines Dept. Inv.* **1963**, 4900.
(4) Lehn, J.-M. *Angew. Chem., Int. Ed. Engl.* **1990**, *29*, 1304.
(5) Lehn, J.-M. *Angew. Chem., Int. Ed. Engl.* **1988**, *27*, 89 and references therein.
(6) Gokel, G. W. *Chem. Soc. Rev.* **1992**, *21*, 39.
(7) Gokel, G. W. *Crown Ethers and Cryptands*; The Royal Society of Chemistry; Cambridge, U.K., 1991.
(8) Schneider, H.-J. *Angew. Chem., Int. Ed. Engl.* **1991**, *30*, 1417.
(9) Ortholand, J.-Y.; Slawin, A. M. Z.; Spencer, N.; Stoddart, J. F.; Williams, D. J. *Angew. Chem., Int. Ed. Engl.* **1989**, *28*, 1394.
(10) Ghadiri, M. R.; Soares, C.; Choi, C. *J. Am. Chem. Soc.* **1992**, *114*, 825.
(11) Turro, N. J.; Burton, J. K.; Tomalia, D. A. *Acc. Chem. Res.* **1991**, *24*, 332.
(12) Hansslinge, L.; Michel, B.; Ringsdorf, H.; Rohrer, H. *Angew. Chem., Int. Ed. Engl.* **1991**, *30*, 569.
(13) Cram, D. J.; Tanner, M. E.; Knobler, C. B. *J. Am. Chem. Soc.* **1991**, *113*, 7717.
(14) Annelli, P. L.; Ashton, P. R.; Ballardini, R.; Balzani, V.; Delgado, M.; Gandolfi, M. T.; Goodnow, T. T.; Kaifer, A. E.; Philip, D.; Petraszkiewicz, M.; Prodi, L.; Peddington, M. V.; Slawin, A. M. Z.; Spencer, N.; Stoddart, J. F.; Vincent, C.; Williams, D. J. *J. Am. Chem. Soc.* **1992**, *114*, 193.
(15) Balzani, V.; Scandola, F. *Supramolecular Photochemistry*; Ellis Harwood Ltd.: Chichester, U.K., 1991; and references therein.
(16) Izatt, R. M.; Eblehardt, L.; Clarke, G. A.; Bruening, R. L.; Bradshaw, J. S.; Cho, M. H.; Christensen, J. J. *J. Sep. Sci. Technol.* **1987**, *2212–3*, 701. Izatt, R. M.; Bruening, R. L.; Bruening, M. L.; Tarbet, B. J.; Krakowiak, K. E.; Bradshaw, J. S.; Christensen, J. J. *Anal. Chem.* **1988**, *60*, 1826. Izatt, R. M.; Pawlak, K.; Bradshaw, J. S.; Bruening, R. *Chem. Rev.* **1991**, *91*, 1721.
(17) Blake, A. B.; Cotton, F. A. *Inorg. Chem.* **1964**, *3*, 5 and references therein.

0020-1669/94/1333-0823$04.50/0

materials used. The complexes were filtered hot to minimize the presence of the hydrate analogous to **2** and the precipitation of microcrystals of **5**. The mixed complexes **6** were prepared by introducing the desired quantities of the 3d metal chlorides into the reaction mixture and recrystallizing the product at least three times, followed by digestion for at least 1 day in an attempt to improve sample homogeneity.

Spectral Measurements and Quantitative Analyses. Powder X-ray diffraction analyses were performed using a Siemens Model D5000 diffractometer. Electronic absorption spectra were recorded on a HP Model 8452A diode array spectrometer using solid samples thoroughly mulled in Nujol. The emission and excitation spectra were recorded on a Perkin-Elmer LS5 luminescence spectrometer in the phosphorescence mode.

Quantitative analyses of copper and zinc were performed on a Perkin-Elmer Model 2380 atomic absorption spectrometer at wavelengths of 242.9 and 213.9 nm, respectively.

Luminescence Decay Rate Constant Measurements. Samples for lifetime measurements were sealed in 4-mm glass tubes, and 77 K measurements were performed with the samples immersed in liquid nitrogen in a 50-mL finger-type EPR quartz dewar. The luminescence decay rate constants were derived from decay curves recorded on our recently acquired apparatus consisting of a Photon Technology International (PTI) PL2300 nitrogen laser (energy = 1.4 mJ/pulse; pulse width < 1 ns) and a matching PL201 dye laser. Excitation of the Mn^{2+} $^4T_1(^4G)$ emitting state at 479 nm was achieved with a coumarin 151 laser dye from Kodak. The luminescence monitoring wavelength was selected using a quarter meter PTI S/N 1137 monochromator with 600 g/mm blazed at 500 nm with $f = 2.5$. The emission was detected by an Hamamatsu R928 photomultiplier tube and then fed into a preamplifier (NE531N from R. S. Components Ltd.) optimized for measurements of decay rate constants between 200 and 10^6 s^{-1}. The amplifier output was sampled by a Tektronix 2232 digital storage oscilloscope of 1000 channels, 100-MHz bandwidth, 100 megasamples/s sampling rate capability, and 8-bit amplitude resolution. The oscilloscope was triggered by a PTI photodiode detector activated by the excitation laser beam. Typically about 1000 transients were averaged by the oscilloscope software and then transferred to a DTK386 20-MHz PC. Eight or ten such transients were further averaged to improve the signal to noise ratio, and the resulting curve was analyzed using the Levenberg–Marquardt nonlinear procedure.[18] Emission intensities were determined from the normalized integrated area under the decay curves. The good performance of the instrumental setup and the in-house least-squares curve-fitting programs was verified using numerous samples analyzed in other facilities. The variable-temperature studies were performed using an Air Products Displex closed-cycle helium refrigerator system with the sample mounted on a copper block with "cryocon grease" as described previously[19] or a custom-built variable-temperature nitrogen gas flow cryostat.

Results and Discussion

Structural Data. The essential details of the crystal structures of **1**–**4** were reported earlier,[1,2] and the structures of **5** are from powder X-ray diffraction patterns similar (Figure 1). Therefore complexes with the general stoichiometry $[(A18C6)_4MCl_4][TlCl_4]_2$, where A = large monovalent cation such as Rb^+ or Tl^+ and M = a 3d element, have isomorphous cubic $F23$ structures. The basic structure is an assembly of $TlCl_4^-$ anions and $[(A18C6)_4MCl_4]^{2+}$ supramolecular species, the latter forming a face-centered cubic sublattice. The $[(A18C6)_4MCl_4]^{2+}$ ions are separated from each other by 14.6 Å and depict well-isolated MCl_4^{2-} species. Interactions among the MCl_4^{2-} ions and between the MCl_4^{2-} and $FeCl_4^-$ (in $TlCl_4^-$ positions) ions are therefore expected to be predominately multipolar.

Competitive Complexation of $MnCl_4^{2-}$ and MCl_4^{2-}. The complexes $[(Rb18C6)_4MCl_4][TlCl_4]_2$ are generally obtained in yields of 60–70% for M = Mn, Co, Cu, and Zn; a low yield was obtained for M = Ni (28%), and the case of the $FeCl_4^{2-}$ ion was complicated by facile oxidation to $FeCl_4^-$. For samples obtained

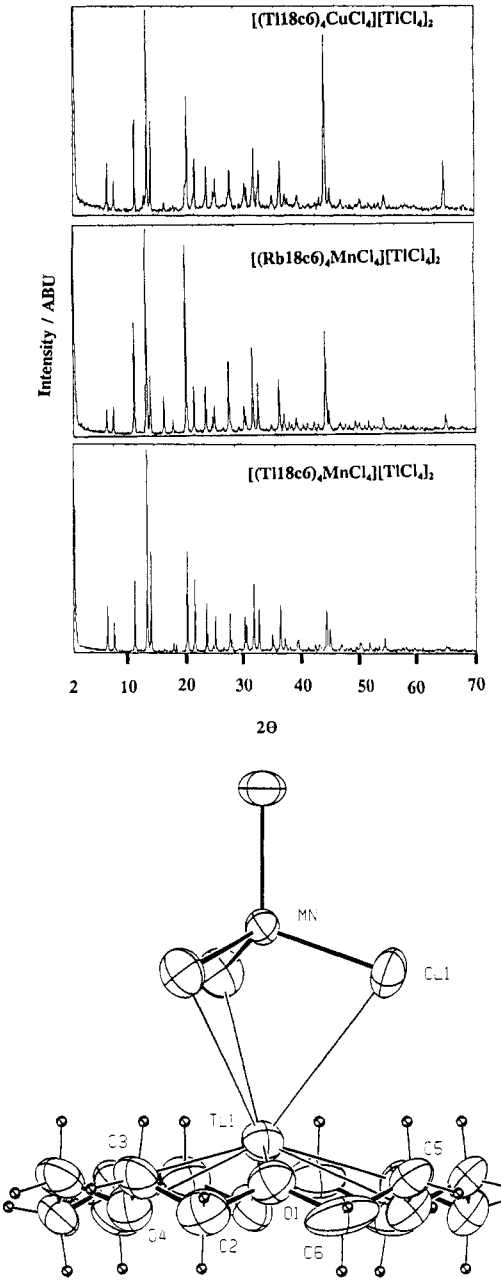

Figure 1. (a) Top: Similar room-temperature powder X-ray diffraction patterns of isostructural $[(A18C6)_4MCl_4][TlCl_4]_2$ complexes. (b) Bottom: Part of the $[Tl18C6)_4MnCl_4]^{2+}$ ion in **3** showing the binding of one of the four $Tl18C6^+$ ions to the T_d $MnCl_4^{2-}$ ligand.

from reaction mixtures to which both Fe^{2+} and Mn^{2+} have been added, the formation of $FeCl_4^-$ was discernible from the inner-filter-effect of its characteristically intense charge-transfer band in the UV region[21] of the $[(Rb18C6)_4MnCl_4]^{2+}$ excitation (vide infra). Samples which were prepared from a mixture of $TlCl_3$ and $FeCl_3$ in the presence of manganese(II) chloride exhibited similar electronic behavior. The $FeCl_4^-$ anions therefore occupy some of the $TlCl_4^-$ 23T sites to give the series $[(Rb18C6)_4MnCl_4][(TlCl_4)_{1-x}(FeCl_4)_x]_2$ (**7**), which is being studied in detail.

When the reaction mixture contains equimolar quantities of Mn^{2+} and M^{2+} (M = Co, Cu), the crystals of **6** (M = Co, Cu) are uniform under microscopic examination but richer in cobalt and depleted of copper, respectively. We have studied this behavior over a wide Cu^{2+} (Table 1) and Co^{2+} (Figure 3) concentration range. The mole fraction of copper incorporated in the crystalline products of **6** (M = Cu) X_6 may be related to

(18) Marquard, D. W. *J. Soc. Ind. Appl. Math.* **1963**, *11*, 431.
(19) Matthews, K. D.; Bailey-Folkes, S. A.; Kahwa, I. A.; McPherson, G. L.; O'Mahoney, C. A.; Ley, S. V.; Williams, D. J.; Groombridge, C. J.; O'Connor, C. J. *J. Phys. Chem.* **1992**, *96*, 7021.
(20) Furlani, C.; Cervone, E.; Valenti, V. *J. Inorg. Nucl. Chem.* **1963**, *25*, 159.
(21) McCuster, P. A.; Scholastica-Kennard, S. M. *J. Am. Chem. Soc.* **1959**, *81*, 2976. Hathaway, B. J.; Holah, D. G. *J. Chem. Soc.* **1964**, 2408. Grinsberg, A. P.; Robin, M. B. *Inorg. Chem.* **1963**, *2*, 817.

Table 1. Relative Mole Fractions of Copper in the Parent Reaction Mixture (X_{RM}) and the Crystalline Product (X_6), 77 K Luminescence Integrated Intensities (I) for the Whole Decay Curves, and Exciton Trapping (K_t) and Migration (K_{DD}) Rates for **6** (M = Cu)

X_{RM}	X_6	K_t, s^{-1}	K_{DD}, s^{-1}	$10^3 I$
0.0	0.00	0	0	2.98
0.05	0.00345	30		3.09
0.02	0.0124	500	20	2.90
0.04	0.0270	460		2.83
0.05	0.0413			2.62
0.10	0.0517		40	2.82
0.08	0.0560	950		2.52
0.15	0.0988	1200		2.11
0.30[a]	0.156			2.85
0.10	0.225	1510	70	1.69
0.50[a]	0.272			1.85
0.30	0.310	1700	90	2.09
0.70	0.320			1.27
0.50	0.350	1310		1.49
0.80	0.462	1970	120	1.14
0.90	0.614	2150	210	0.744
0.90	0.76	2470	950	0.620

[a] Compounds of $[(Tl18C6)_4MnCl_4]^{2+}$.

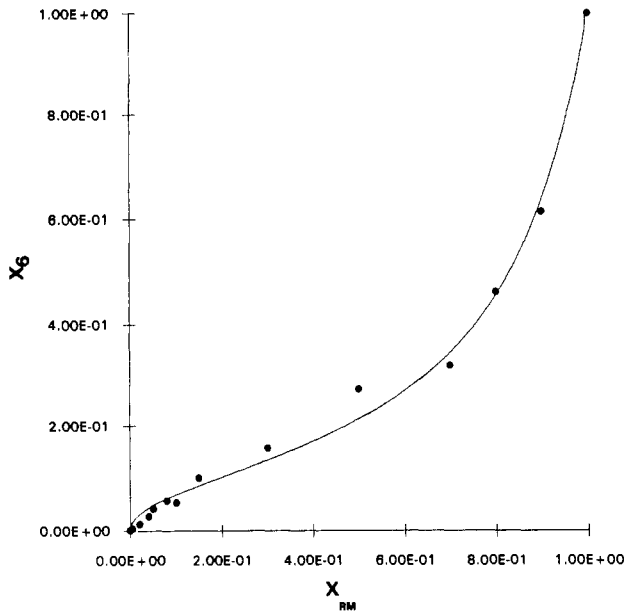

Figure 2. Dependence of the mole fraction (X_6) of guest copper in the final crystalline host products **6** (M = Cu) on the initial mole fraction of copper(II) (X_{RM}) and manganese(II) ($1 - X_{RM}$) in the mother reaction mixture.

that of Cu^{2+} used in the parent reaction mixture (X_{RM}) by eq 1,

$$X_6 = k_1 X_{RM}{}^a/(k_1 X_{RM}{}^a + k_2(1 - X_{RM})) = X_{RM}{}^a/(X_{RM}{}^a + k_2/k_1(1 - X_{RM})) \quad (1)$$

where k_1 and k_2 are the cation discrimination indices[22] of Cu^{2+} (or Co^{2+}) and Mn^{2+}, respectively, and a is an empirical parameter. The best fit of the experimental data (Figure 2) was obtained with a square root dependence on the concentration of Cu^{2+} ($a = {}^1/_2$), a linear dependence on the concentration of Mn^{2+} ($1 - X_{RM}$), and the ratio $k_2/k_1 = 5$. The nonlinear dependence of X_6 on the concentration of copper available in the reaction mixture (X_{RM}) is not surprising in view of the numerous geometries available to the tetrachlorocuprate anion and the unfavorable

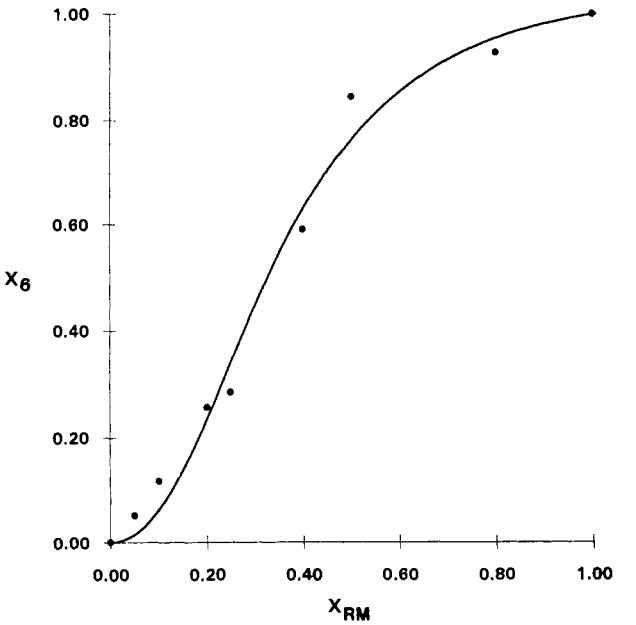

Figure 3. Dependence of the mole fraction (X_6) of guest cobalt in the final crystalline host products **6** (M = Co) on the initial mole fraction of cobalt(II) (X_{RM}) and manganese(II) ($1 - X_{RM}$).

tetrahedral restrictions[23] of the cubic $F23$ assembly adopted by **1–7**. Whereas this view is plausible for Cu^{2+}, the possible dependence of k_2/k_1 on X_{RM}, which could then lead to nonunity exponents, cannot be ruled out; this may indeed be the case for the Co/Mn system for which a square dependence of X_6 in **6** (M = Co) on X_{RM} is observed (Figure 3).

Attempts to dope $MnCl_4^{2-}$ in **5** (M = Zn) required a large excess of manganese chloride (over three times that of zinc chloride) to obtain marginal yields of products with detectable but very weak emission from $MnCl_4^{2-}$. This weak emission followed normal decay kinetics (vide infra). These results suggest that $ZnCl_4^{2-}$ ions are decisively preferred for incorporation in **6** (M = Zn) over $MnCl_4^{2-}$. For **6** (M = Ni, $X_{RM} = 0.02$), crystals of the light yellow phase of mostly $[(Rb18C6)_4MnCl_4][TlCl_4]_2$ are deposited first followed by an epitaxial growth of the blue-green $[(Rb18C6)_4NiCl_4][TlCl_4]_2$ phase. The two regions of the individual crystals are readily observed by optical microscopy, and shaking the crystals in methanol or ethanol dissolves the blue-green phase leaving **5** (M = Mn). Since nonuniform doping was evident, no further studies of this system were undertaken.

The above competitive binding results are qualitatively consistent with the trend of the thermodynamic stabilities of MCl_4^{2-} anionic ligands[17] relative to $MnCl_4^{2-}$. The $NiCl_4^{2-}$ anion is less stable than $MnCl_4^{2-}$ by $\approx$57 kJ/mol while $ZnCl_4^{2-}$ is the more stable anion by $\approx$26 kJ/mol. The $CuCl_4^{2-}$ ion is estimated to be $\approx$21 kJ/mol less stable than the $MnCl_4^{2-}$ anion although, by another estimate, it could be the more stable anion by $\approx$11 kJ/mol.[17] The preferential incorporation of $MnCl_4^{2-}$ into **6** (M = Cu) compared to $CuCl_4^{2-}$ ($k_2/k_1 = 5$) now confirms the greater stability of $MnCl_4^{2-}$ anions. The $CoCl_4^{2-}$ anion is estimated to be $\approx$10 kJ/mol less stable than $MnCl_4^{2-}$ or, by another estimate,[17] as stable as $MnCl_4^{2-}$. Incorporation of $CoCl_4^{2-}$ in **6** (M = Co) is preferred to $MnCl_4^{2-}$ (Figure 3); the best fit to eq 1 is obtained with a square dependence ($a = 2$) on X_{RM} and the ratio $k_2/k_1 \approx 0.14$. Since crystallization of **1–7** is by the foregoing evidence occurring under strict thermodynamic control, we must conclude that $CoCl_4^{2-}$ is more stable than $MnCl_4^{2-}$ and that the relative stabilities of MCl_4^{2-} anions follow the sequence $ZnCl_4^{2-} > CoCl_4^{2-} > CuCl_4^{2-} > NiCl_4^{2-}$.

(22) Matthews, K. D.; Fairman, R. A.; Johnson, A.; Spence, K. V. N.; Kahwa, I. A.; McPherson, G. L.; Robotham, H. *J. Chem. Soc., Dalton Trans.* **1993**, 1917.

(23) Deeth, R. J. *J. Chem. Soc., Dalton Trans.* **1990**, 355. Lohr, L. L.; Lipscomb, W. H. *Inorg. Chem.* **1963**, *2*, 911. Desjardins, S. R.; Penfield, K. W.; Cohen, S. L.; Musselman, R. L.; Solomon, E. I. *J. Am. Chem. Soc.* **1983**, *105*, 4590.

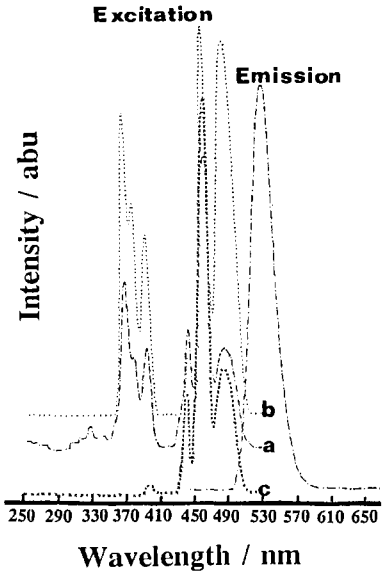

Figure 4. 77 K excitation (emission monitored at 535 nm) and emission (excitation at 350 nm) spectra for $[(Rb18C6)_4MnCl_4]^{2+}$ ions at 77 K: (a) $[(Rb18C6)_4MnCl_4][TlCl_4]_2$; (b) $[(Rb18C6)_4\{(MnCl_4)_{1-x}(CuCl_4)_x\}][TlCl_4]_2$ (x = 0.056); (c) $[(Rb18C6)_4MnCl_4][(TlCl_4)_{1-x}(FeCl_4)_x]_2$.

Luminescence of $[(Rb18C6)_4MnCl_4]^{2+}$. The emission and excitation spectra of **3** at 77 and 298 K are similar to those of **5** (M = Mn) and are typical of T_d $MnCl_4^{2-}$ ions[24,25] (Figure 4a). For **6** (M = Cu), charge-transfer bands ($^2E \leftarrow {}^2B_2$) (27 000–30 000 cm^{-1}) and $^2A_2 \leftarrow {}^2B_2$ and $^2E \leftarrow {}^2B_2$ (21 000–23 000 cm^{-1})[1,23] of $CuCl_4^{2-}$ exert a dominant inner-filter-effect[26] on the d–d transition of $MnCl_4^{2-}$ (Figure 4b). The most efficient excitation of $MnCl_4^{2-}$ ions in **6** (M = Cu) is therefore via the $^6A_1 \rightarrow {}^4T_1$ (^4G) absorption which peaks at about 485 nm. This transition is also appropriate for $[(Rb18C6)_4MnCl_4][(TlCl_4)_{1-x}(FeCl_4)_x]_2$ complexes in which the charge-transfer transition of the $FeCl_4^-$ ion in the near-UV exerts a more intense inner-filter-effect (Figure 4c). For comparative purposes all photophysical investigations were carried out with excitations at 479 nm and emission monitored at 535–570 nm.

Energy Migration on the $[(Rb18C6)_4MnCl_4]^{2+}$ Sublattice (A = Rb, Tl). The luminescence decay rates of $MnCl_4^{2-}$ in $[(A18C6)_4MnCl_4]^{2+}$ at 77 K (≈330 (A = Rb) and ≈360 (A = Tl) s^{-1} are significantly faster than the rates reported for uncoordinated $MnCl_4^{2-}$ ions (250–270 s^{-1}). This is due to Rb–Mn and Tl–Mn spin–orbit coupling[24] and polarization effects[27] of the $A18C6^+$ ions which are expected to lead to increased decay rates of $MnCl_4^{2-}$ excitation.

The decay curve of the $[(Rb18C6)_4MnCl_4]^{2+}$ ion in **5** (M = Mn) is exponential at 77 K, but slight deviations from strict exponential behavior are reproducibly (three samples by three different people) found at 297 K after about 3 lifetimes. Rate constants of 330 and 830 s^{-1}, respectively, were extracted at 77 and 298 K, respectively, from the exponential parts. Doping with Zn^{2+} [**6** (M = Zn, X_6 = 0.05)] yields samples with exponential luminescence decay kinetics at 77 K and, excepting slight deviations after about 3 lifetimes, 297 K; but the decay rate constants are in this case 330 and 450 s^{-1}, respectively. A zinc sample doped with small amounts of $[(Rb18C6)_4MnCl_4]^{2+}$ species (**6** (M = Zn, $X_6 \approx 1$) also exhibits similar exponential luminescence

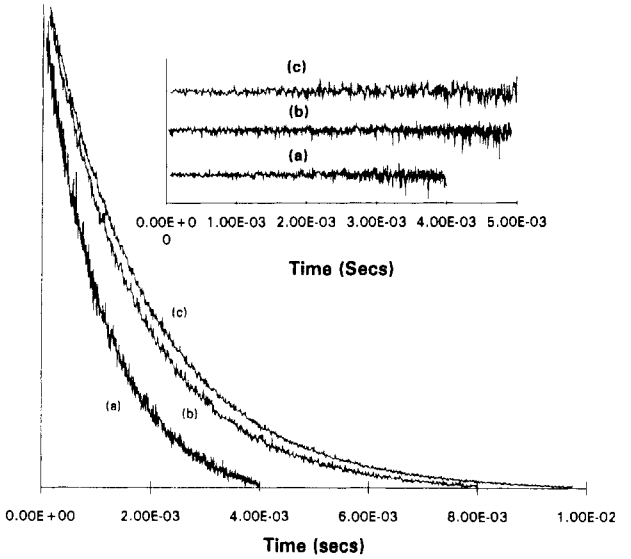

Figure 5. 298 K decay curves of **5** (M = Mn) (a) and **6** (M = Cu (X_6 = 0.003); M = Zn (X_6 = 0.05)) showing the scattering effects of Cu (b) and Zn (c). (See text on $MnCl_4^{2-}$ excitation.) The inset shows weighted residuals for exponential fits.

decay kinetics with rate constants of 310 (77 K) and 460 s^{-1} (room temperature), respectively. The faster nonexponeital luminescence decay behavior at 298 K exhibited by **5** (M = Mn) is consistent with tandem energy migration/trapping at the $[(Rb18C6)_4MnCl_4)^{2+}$ sublattice. The traps appear to populate the matrix of **5** (M = Mn) in such a sparse fashion that introduction of $[(Rb18C6)_4MCl_4]^{2+}$ or $[(Tl18C6)_4MCl_4]^{2+}$ (M = Cu, Zn), scatterers[28] in the cubic three-dimensional array of $[(Rb18C6)_4MnCl_4)^{2+}$ donors, reduces the donor–acceptor transfer rate substantially (Figure 5). For a better understanding of the energy migration/trapping processes, we have studied the temperature evolution of the luminescence decay constants of **3**, **5** (M = Mn), and **6** (M = Zn, X_6 = 0.05).

The decay rate constant exceeds the spontaneous rate at $T >$ 200 K for **5** (M = Mn) and $T >$ 190 K for **3**. The observed rate constant for **3** and **5** (M = Mn) (k_o) is given by eq 2, in which

$$k_o = k_{mt} + k_c \qquad (2)$$

k_{mt} = decay rate constant due to tandem energy migration/trapping and k_c = cumulative rate constant that includes all other contributions. The values of k_c may be taken to be equal to the rate constants for **6** (M = Zn, X_6 = 0.05) measured under the same conditions employed for the determination of k_o. The values of k_o, k_c, and k_{mt} so derived are given in Table 2 for various temperatures, and the corresponding Arrhenius plot (Figure 6a) gives the thermal barrier to the trapping process of ΔE = 48 ± 2 kJ mol^{-1} and pre-exponential factor of 8.2×10^{10} s^{-1}. For **3**, k_o is much larger compared to that of **5** (M = Mn) and a simple plot of ln k_o vs $1/T$ provides ΔE = 46 ± 3 kJ mol^{-1} and a preexponential factor of 2.8×10^{13} s^{-1} (Figure 6b). Water, by virtue of its large dipole moment, is a well-known efficient luminescence quencher for strong phosphors such as Eu^{3+} and Tb^{3+}.[29,30] If small amounts of hydrate **2a** are trapped in a **5** (M = Mn) lattice, luminescence quenching facilitated by multipolar coupling of electronic states of Mn^{2+} with vibrational modes of the water molecules is possible. A rubidium "wet" sample **5** (M

(24) Writon, M.; Ginley, D. *Chem. Phys.* **1974**, *4*, 295. Presser, N.; Ratner, M. A.; Sundheim, B. R. *Chem. Phys.* **1978**, *31*, 281. Buric, I.; Nikolac, K.; Aleksic, A. *Acta Phys. Pol.* **1986**, *A69*, 561. Marco de Lucas, M. C.; Rodriquez, F. *J. Phys. Condens. Matter* **1989**, *1*, 4251.
(25) Cotton, F. A.; Goodgame, D. M. L.; Goodgame, M. *J. Am. Chem. Soc.* **1962**, *84*, 167. Furlani, C.; Furlani, A. *J. Inorg. Nucl. Chem.* **1961**, *19*, 51. Foster, J. J.; Gill, N. S. *J. Chem. Soc. A* **1968**, 2625.
(26) Kirk, A. D.; Schlaffer, H.-L. *J. Chem. Phys.* **1970**, *52*, 2411.
(27) Mason, S. F.; Peacock, R. D.; Stewart, B. *Chem. Phys. Lett.* **1974**, *29*, 149.
(28) Karlen, T.; Ludi, A.; Gudel, H. U.; Rienen, H. *Inorg. Chem.* **1991**, *30*, 2249. Auberbach, R. A.; McPherson, G. L. *Phys. Rev.* **1986**, *33*, 6815 and references therein. Blasse, G.; Bril, A. *Philips Techn. Rev.* **1970**, *31*, 303. Blasse, G.; Bril, A. *Recl. Trav. Chim. Pays-Bas* **1986**, *105*, 143.
(29) Harrocks, W. deW., Jr.; Sudnick, D. R. *Acc. Chem. Res.* **1981**, *14*, 384.
(30) Harrocks, W. deW., Jr.; Albin, M. *Prog. Inorg. Chem.* **1984**, *31*, 1. Hall, C.; Dennis, C.; Sharpe, N. W. *J. Photochem. Photobiol. A* **1990**, *52*, 365.

Table 2. Temperature Evolution of the Luminescence Decay Rate Constant (s^{-1}) of $[A18C6)_4MnCl_4]^{2+}$ Emission for **6** (A = Rb, M = Zn, X_{RM} = 0.05) (k_c), **5** (A = Rb, M = Mn) (k_o), and **3** (A = Tl) (k^1)[a]

T, K	k_o	k'	k_c	k^1_{mt}	k^2_{mt}
77	330	360	310		
160	300				
176		370			
188		380			
196		400			20[b]
199	310		330		
220	300				
226		730			380[b]
240	320				
251	330		330		
260		21740			21390
266	360		330	30[b]	
270		31450	340		31070
277	440		360	80	
289	590		420	170	
299	830		470	360	

[a] The corresponding trapping rates due to migration are k^1_{mt} (A = Rb) and k^2_{mt} (A = Tl). [b] k_c = 330 s^{-1} (A = Rb) at T < 250 K and 380 s^{-1} (A = Tl) at T < 260 K.

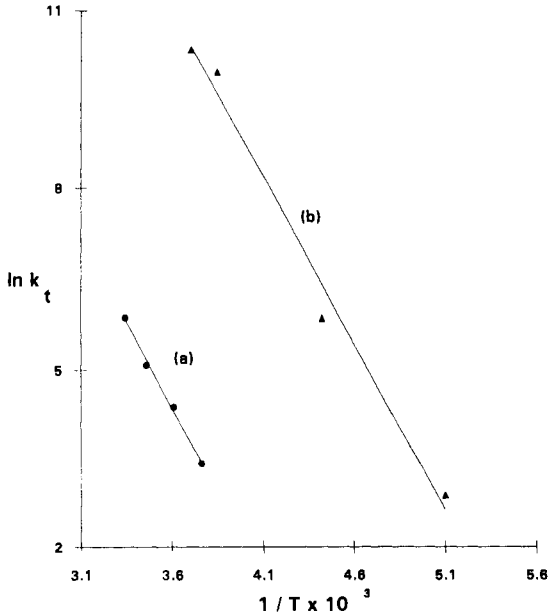

Figure 6. Temperature evolution of exciton trapping constants, k_{mt}, for $[(A18C6)_4MnCl_4][TlCl_4]_2$ (A = Rb (a), Tl (b)).

= Mn) harvested from a cold reaction mixture to which water had been added and the solution–crystal contact maintained for 1 week exhibits dramatically faster decay kinetics at room temperature (Figure 7a). If the "wet" sample is freeze dried before analysis (Figure 7b), typical decay behavior of **5** (M = Mn) (vide supra) is observed. We therefore conclude that water molecules are the most efficient traps of excitation energy of $[(A18C6)_4Mn]^{2+}$ in the lattices of **3** and **5** (M = Mn). The hydrate $[(Rb18C6)_4MnCl_4][TlCl_4]_2 \cdot 0.25H_2O$ and the anhydrate **5** (M = Mn) might occur simultaneously within the same crystals since separate phases are obtained when both species are present in large quantities.[1] The temperature dependence, however, is not explained by multiphonon relaxation processes involving water since significant differences between multiphonon relaxation model predictions[31] and the observed temperature dependence were obtained. We attribute the thermal barrier to the effect of dynamic crown ether reorientations that are known to occur at

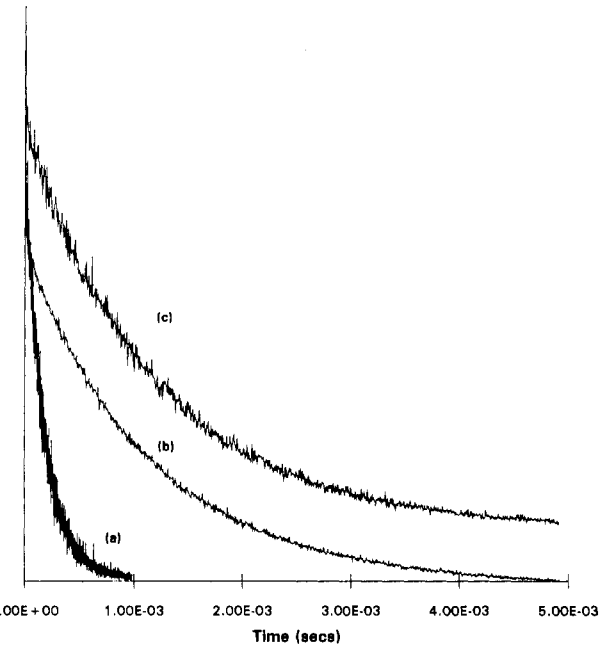

Figure 7. 298 K decay curves of **5** (M = Mn) showing the effect of water on the $MnCl_4^{2-}$ emission: (a) "wet" sample; (b) typical sample isolated from warm mother liquor; (c) "wet" sample freeze dried before analyses.

temperatures above 200 K and show thermal barriers of the same order of magnitude (31–55 kJ mol^{-1}).[32] These reorientations were recently confirmed crystallographically in a comparative study of the cryogenic and room-temperature structures of **4**.[33] The crown ether reorientational motion possibly introduces a dynamic noncentrosymmetric crystal field at $MnCl_2^{2-}$ which enhances the $MnCl_4^{2-}$–water energy-transfer probability. The higher preexponential factor for **3** is most probably due to a larger water content compared to that of the rubidium analogue **5** (M = Mn).

Luminescence Decay Dynamics of $[(Rb18C6)_4MnCl_4]^{2+}$ in 6 (M = Cu). The complexes **6** (M = Cu) are luminescent at 297 K when $0 < X_6 < 0.1$ and at 77 K for $0 < X_6 < 0.76$. The decay curves obtained at 77 K are essentially exponential up to large copper concentrations ($0 < X_6 < 0.22$) and nonexponential for $X_6 > 0.23$. The decay rate constants extracted from the exponential curves ($X_6(Cu) < 0.23$) show a modestly increasing trend with increasing copper concentration while the integrated intensities (Figure 8) increase with the square of the manganese concentration ($1 - X_6(Cu)$). Since large quantities of Cu^{2+} are required to achieve nonexponential behavior, one-dimensional energy transfer is not important.[27] Three-dimensional energy migration is a reasonable expectation following the cubic nature of the $[(Rb18C6)_4MnCl_4]^{2+}$ donor assembly.[1] At the lower concentrations of the $[(Rb18C6)_4CuCl_4]^{2+}$ exciton acceptors (**6**, M = Cu and $0 < X_6 < 0.22$), the system is essentially in the dynamic limit described by Huber,[34] while at high concentrations the model which is intermediate between the dynamic and static[35] limits applies. The direct donor–acceptor transfer rate K_{DA} can be derived from a plot of the trapping rate constants K_t, obtained from the observed early time exponential decay rates (K_{et}) using eq 3. Equation 4 may now be used to calculate the donor–acceptor $\{[Rb18C6)_4MnCl_4]^{2+}$–$[(Rb18C6)_4CuCl_4]^{2+}\}$ coupling constant (α) assuming dominant Dexter–Foster type dipole–dipole interactions,[36] where R = donor–acceptor distance of closest approach

(31) Reed, E. D., Jr.; Moos, H. W. *Phys. Rev.* **1973**, *B8*, 980. Riseberg, L. A.; Gandrus, W. B.; Moos, H. W. *Phys. Rev.* **1967**, *159*, 262. Reed, E. D., Jr.; Moos, H. W. *Phys. Rev.* **1973**, *B8*, 9880. Partlow, W. D.; Moos, H. W. *Phys. Rev.* **1967**, *157*, 252. Riseberg, L. A.; Moos, H. W. *Phys. Rev.* **1968**, *174*, 429.

(32) Buchanan, G. W.; Morat, C.; Ratcliffe, C. I.; Pipmeester, J. A. *J. Chem. Soc., Chem. Commun.* **1989**, 1306.

(33) Fender, N. S.; Finnegan, S. A.; Miller, S.; Mitchell, M.; Kahwa, I. A.; Fronczek, F. R. Submitted for Publication. Dawes, S. B.; Ward, D. L.; Fussa-Rydel, O.; Huang, R. H.; Dye, J. L. *Inorg. Chem.* **1989**, *28*, 2132.

(34) Inokuti, M.; Hirayama, F. *J. Chem. Phys.* **1965**, *43*, 1978.

(35) Yokota, M.; Tanimoto, O. *J. Phys. Soc. Jpn.* **1967**, *22*, 779.

(36) Dexter, L. *J. Chem. Phys.* **1953**, *21*, 836. Foster, T. Z. *Naturforsch.* **1949**, *49*, 321.

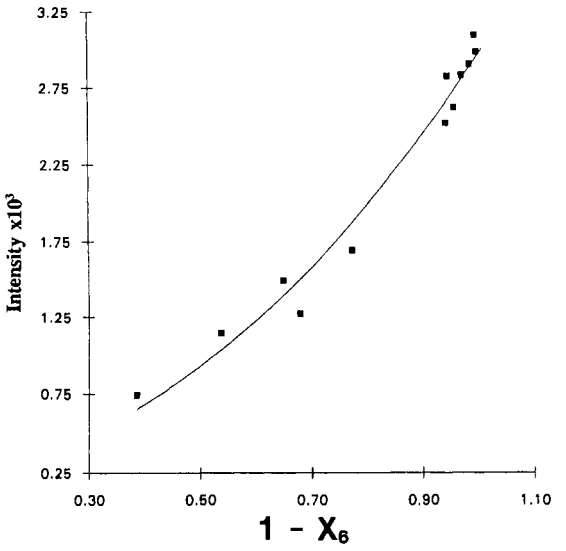

Figure 8. Dependence of the luminescence integrated intensity of $[(Rb18C6)_4MnCl_4]^{2+}$ on the concentration of manganese in **6** (M = Cu) $(1 - X_6)$.

$$K_t = K_{et} - K_c \tag{3}$$

$$K_{DA} = \alpha/R^6 \tag{4}$$

(i.e. 14.6 Å for **1–6**) and K_{DA} is the asymptotic limiting transfer rate (K_t at $X_6 \approx 1$) (Figure 9). Using $K_{DA} = 2700\ s^{-1}$, eq 3 yields $\alpha = 2.42 \times 10^{-50}\ m^6\ s^{-1}$.

Trapping rates due to energy migration, K_{DD}, may be derived from the long time ($I(t) \approx 0.01I(o)$) exponential decay rates (K_{1t}) (Table 1 and Figure 9) using eq 5. The parameter K_c is

$$K_{DD} = K_{1t} - K_c \tag{5}$$

the cumulative decay rate in the absence of copper measured under the same conditions as K_{1t}. Equations 6 and 7 can be

$$K_{DD} = 21N_A N_D \alpha^{1/4}\beta^{3/4} \tag{6}$$

$$K_D = 20N_A N_D \alpha^{1/2}\beta^{1/2} \tag{7}$$

employed to determine the donor–donor coupling constant β assuming the diffusion and hopping models, respectively,[37] for the concentration range in which K_{DD} is proportional to the product of the concentrations of copper and manganese ($0 < X_6 < 0.46$) (Figure 10). In eqs 6 and 7 N_A and N_D are the number of acceptors and donors per cubic meter, respectively. For a sample of **6** (M = Cu, $X_6 = 0.0124$) the diffusion model yields $\beta = 1.1 \times 10^{-52}\ m^2\ s^{-1}$, while the hopping model gives $\beta = 8.2 \times 10^{-54}\ m^6\ s^{-1}$. With either model α is ≈2–3 orders of magnitude greater than β; therefore, the diffusion model is more appropriate. Not surprisingly, however, fitting the full decay curve of the samples exhibiting nonexponential decay behavior to the Yokota–Tanimoto expression[35] yielded poor agreement between the calculated and observed decay curves, clearly showing that this model is not suitable for this system.[38]

The luminescence decay curves of **6** (M = Cu, $X_6 < 0.05$) measured at 297 K are exponential up to 3 lifetimes; noticeable derivations from strict exponentiality are observed at longer times after the excitation pulse. The intensities are, however, so low

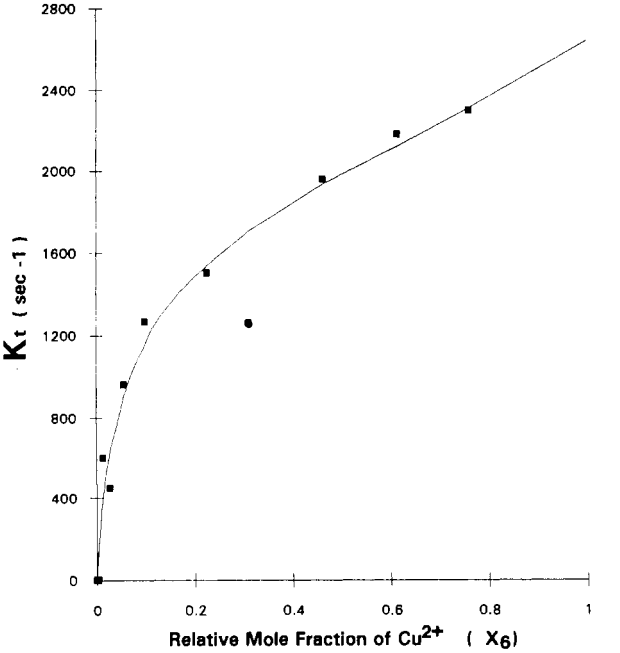

Figure 9. Dependence of the donor–acceptor transfer rate (K_t) on the copper (acceptor) concentration (X_6) in **6** (M = Cu).

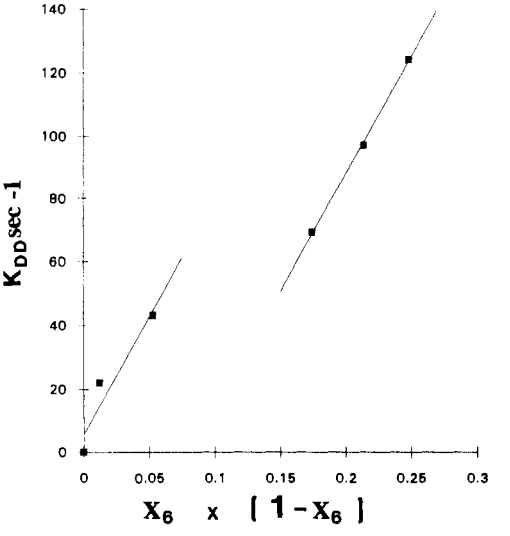

Figure 10. Dependence of the trapping rate due to energy migration (K_{DD}) on the concentrations of both copper and manganese in **6** (M = Cu).

that at X_6(Cu) ≈ 0.05 emission is already too weak to measure. $CuCl_4^{2-}$ is an excellent trap of $MnCl_4^{2-}$ excitation at 297 K; the observed emission originates from $MnCl_4^{2-}$ and too far from $CuCl_4^{2-}$ for efficient coupling. For this type of emission the $CuCl_4^{2-}$ ions are effectively scatterers of $MnCl_4^{2-}$ excitation which would otherwise be quenched by water. Accordingly the 298 K decay rates, extracted from the exponential parts, decrease modestly from 560 to 470 s^{-1} while X_6 is increasing from 0.3 to 5.6%, respectively.

Acknowledgment. We thank the Postgraduate and Research and Publication Committees of UWI for funds to purchase the laser facilities. We also thank The Royal Society of Chemistry and The Third World Academy of Sciences for financial support. The variable-temperature data for **5** (M = Mn) was acquired by I.A.K. during a visit with Professor Gary L. McPherson at Tulane University; the operational amplifier used was designed by Professor Colin D. Flint and built by Mr. P. O'Grady (Birkbeck College).

(37) Bettinelli, M.; Flint, C. D. *J. Phys. Condens. Matter* **1991**, *3*, 4433. Huber, D. L. *Phys. Rev.* **1979**, *B20*, 2307. Huber, D. L. *Phys. Rev.* **1979**, *B20*, 5333. Weber, M. J. *Phys. Rev.* **1967**, *157*, 262. Buijs, M.; Blasse, G. *J. Lumin.* **1988**, *39*, 323.
(38) Chow, H. C.; Powell, R. C. *Phys. Rev. B.* **1980**, *21*, 3785.